International Journal of Applied Engineering Research ISSN 0973-4562 Volume 12, Number 8 (2017) pp. 1529-1535

Investigation Testing of Structural Members of Large-sized Reconfigurable Spacecraft Antenna Reflectors

Mikhail Viktorovich Boyarchuk, Sergey Alekseevich Gusev, Igor Vladimirovich Teminovskiy, Valeriy Yuryevich Terekhov

Interdisciplinary Engineering Center for Composite Materials, Bauman State Technical University, Moscow, Russia

Abstract

Objectives: The relevance of the article is associated with the need for large-sized reconfigurable reflectors to solve a number of problems in the field of navigation, telecommunications, and the study of other planets. The purpose of research is to assess the rationality of using carbon fiber power rod structure members and ropes made of polymeric materials in the reconfigurable antenna design, in terms of the reflective surface quality in space conditions.

Methods: Investigative testing of power rod structure members to determine the CLTE is carried out in the climate chamber using strain gauges, which are glued to the sample surface. Structural test polymeric ropes were performed using deformometer and special grippers.

Findings: This article describes testing of structural elements of large-sized reconfigurable spacecraft antenna reflectors. The description is given for the studied testing objects, the conditions under which the tests were conducted and the test equipment. The studies resulted in the determined CLTE of power rod elements made of carbon fiber plastic based on carbon threads and ECD-MD binder, and strength characteristics of the polymeric ropes made of Armos aramid fibers. The uniqueness of the research is in conducting tests for these combinations of composite materials.

Improvements/Applications: In terms of practical significance, the research clearly indicates that these power rods and ropes are suitable for exploitation in the outer space as structural members of large-sized reconfigurable spacecraft antenna reflectors.

Keywords: Composite Materials, Spacecraft, Large-Sized Reflector, Polymeric Ropes

INTRODUCTION

Advanced spacecraft (SC) designed for solving tasks in the sphere of communication, navigation, exploration of natural resources of the Earth, studying planets, their satellites and other celestial bodies should be equipped with more and more improved space antennas.[1-2] In this regard, mirror antennas with rigid permanent or flexible controlled reflector configuration, as well as those deployable in space with reconfigurable reflectors of petal, umbrella or rim (membrane-cable) type, have great potential.[3] Antenna performance (number of beams, pointing accuracy) increases along with the reflector surface area, but simultaneously complexity of meeting the reflecting surface profile accuracy requirements increases, as well.[4-5]

When creating mirror space antenna reflectors, the most complicated task is to provide high stability of the reflector form and dimensions in changing temperatures and temperature drops in the process of SC orbital motion. Permissible tolerance of form and dimensions should not exceed the value of $\Lambda/16$-$\Lambda/50$, where Λ is the radio emission wavelength. Within the range of radio frequencies L, where reconfigurable reflectors are primarily used, these deviations make 4 to 14 mm. A reconfigurable reflector should be compactly packed under a launch vehicle fairing, which diameter in most cases does not exceed 4 m. An obvious complex interdisciplinary technical problem is plain to see that is related to unfolding and hardening of multi-link reconfigurable structure of significantly bigger diameter than the diameter of a fairing. It is clear that with the increase of the aperture diameter it will be more and more complicated to meet the accuracy requirements for maintaining defined form and dimensions.[6-7]

A great role in providing a radio-reflecting surface accuracy is played by the structure dimension stability in space conditions, where temperature reaches such values as +150°C and -170°C.

The explored objects are parts of a large-sized reconfigurable antenna reflector, in particular: power rod structure members, polymer composite ropes.

These investigation tests of structure members of large-sized reconfigurable spacecraft antenna reflectors have not yet been performed because they are confined to certain materials and items. Annually huge number of tests focused on defining thermal and strength properties are performed in various spheres of human activity worldwide. Some publications provide tests aimed at definition of thermal properties of carbon composite materials.[8] Tests intended to determine the effect of carbon fiber on thermal properties of graphene foam, and to study the properties of spiral carbon fibers[9-10] are being performed.

The study focuses on the materials used in space for spacecraft structures, as well as on phenolic ablation materials for re-entry vehicles.[11-12]

CONCEPT HEADINGS

1. The targets of the research are tubular samples made of carbon composite based on carbon threads and ECD-MD binding oligomer (chlorine containing epoxy resin). The samples were carbon composite straight fixed length pipes with internal diameter 60 mm and thickness from 6 mm to 6.5 mm with occasional thickenings up to 7 mm. Nominal scheme of the samples reinforcement is (0°/±45°/90°)2/(90°/±45°/0°)2, i.e. on average it should be the material which is quasi-tropic with regard to X0Y axes, where axis 0X goes along the straight generating line and axis 0Y goes along the circle. Laying the threads is symmetrical with regard to median surface. In theory the properties of such material along axes 0X and 0Y should be identical. However, during the heating up and cooling of the tubular samples made of composite materials, it should be noted that the coefficient of linear thermal expansion (CLTE) of the material in the direction of the wall thickness (in 0Z direction) is significantly higher than in 0X and 0Y directions, which leads to thermal stresses in 0Y and 0Z directions. Thus, the circumferential strain on the sample surface will depend not only on average Coefficient of Linear Thermal Expansion in the circumferential direction, but also on thermal stresses thickness distribution.[13]

Testing was performed on two samples. The external surface of the samples features significant irregularities that lead to thickness fluctuations (Figure 1).

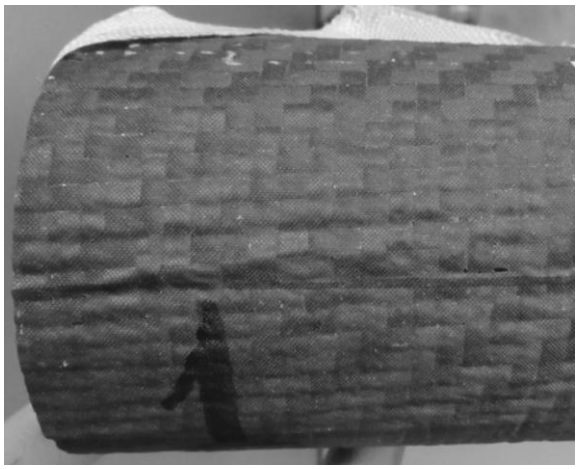

Figure 1: View of the sample surface

During heating–cooling of the tubular samples two coefficients of thermal expansion (α_x and α_y) along each of the orthotropy axes of the tubular samples can be defined based on deformations level on the external surface. With neglect of the impact of thermal stresses related to significant anisotropy of the Coefficient of Linear Thermal Expansion and of the rigidity in-plane and crosswise of the reinforcement plane, for the tubular samples in question $\alpha_x \approx \alpha_y$, however, their actual values may significantly vary. Notably, these variations are related not only to the above-mentioned thermal stresses but also to the impact of non-homogeneity of the material structure on the sample surface. As the experience of composites study shows, the Coefficients of Linear Thermal Expansion are more sensitive to deviations of the fibers laying angles as well as to fluctuations of the content of the binder and microporosity than to the rigidity properties.

Thus, in the process of experimental study it is necessary to determine both α_x and α_y.

In order to define the Coefficient of Linear Thermal Expansion TKF01-5-200 type (base 5 mm) tension gauges were glued on the samples near the central cross-section in the areas located at 120° along the circle: one longitudinal and one transverse per each area (Figure 2). Upon conducting two tests two more circular FLA-5-11 type sensors were glued on sample No.2 for additional control (base 5 mm) (Figure 3).

Prior to attaching the sensors in the areas of their allocation the samples surface was flattened out with the help of cold curing polymer adhesive: attaching the adhesive on the surface with subsequent flattening out the surface after the adhesive polymerization (Figure 2–Figure 4).

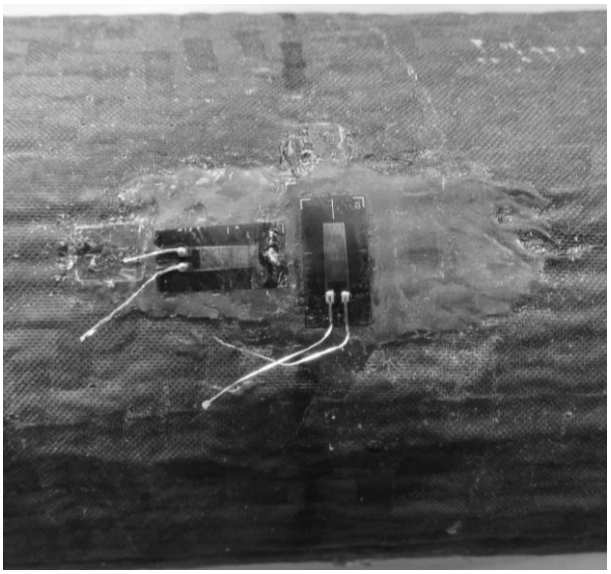

Figure 2. One of the areas of TKF01-5-200 type sensors attachment

Figure 3. One of the areas of attachment of the sensors of two types

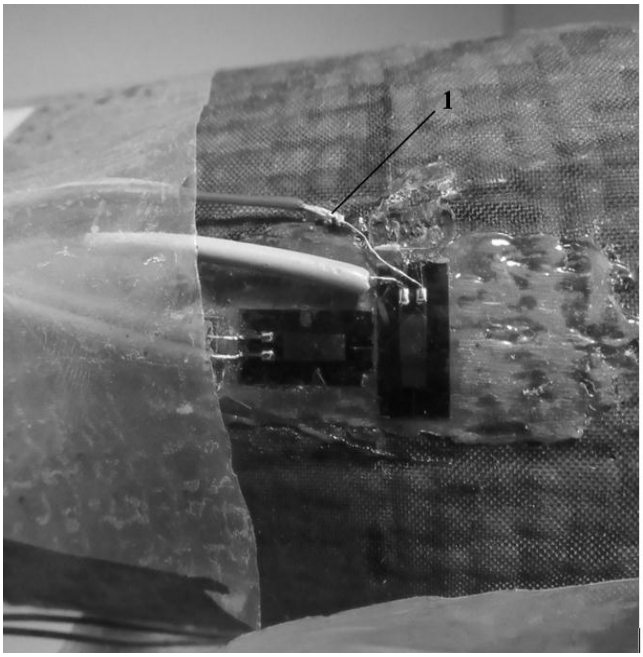

Figure 4. The peculiarities of connecting the sensors with the wires of the registering device (1 – seam area, insulation sleeve is moved)

Further on, the peculiarity of the registering device wires connection with the sensor leads is shown: it has minimal amount of soldering alloy and does not involve applying the transition element (weldolets), glued on the sample for the force stress testing, because the presence of weldolets containing a significant amount of metal may lead to distortion of the deformations field during temperature influence (Figure 3).

In order to prevent the sensors damage the wires connecting the sensors with the registering device SIIT-3 are glued on the samples with the stripes of scotch tape. The compensatory sensors are glued on the ceramic plates with the Coefficient of Linear Thermal Expansion equal to $0.6 \cdot 10^{-6}$ (1/°C).

When studying tubular samples in question the deformations in the direction of orthotropy axes 0X and 0Y are similar in value, that is why it is possible to neglect the impact of the tension gauges' Coefficient of Linear Thermal Expansion on the testing results.

Three tests of the samples with periodic registration of all the tension sensors readings were performed in a climatic chamber. Each test involved two cycles "heating – cooling" in temperature range from –30°C to +60°C. Further on, a typical dependency of the temperature change on time is displayed, together with the readings of one of the sensors (Figure 5). It is seen here that after reaching the target temperature the exposure time was taken at this temperature in order to provide for heating the samples material. During the tests humidity was maintained at the level of 40 – 50%.

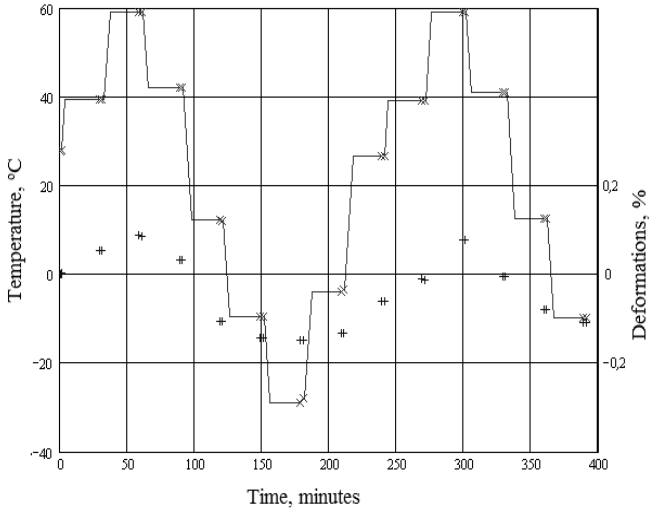

Figure 5. Dependency of temperature on time during the tests (red lines and symbols) and on deformation based on sample No.2 sensor 5 readings (blue symbols)

During all the tests readings of two longitudinal and three transverse sensors were registered at the first sample. During all the tests readings of three longitudinal and two transverse sensors were registered at the second sample, and during the third test – of the two additional transverse sensors, as well.

2. Conducting investigation tests of the structure members of spacecraft large-sized reconfigurable antenna reflectors – ropes made of polymer materials.

Test specimens of yarns made of Armos aramid fibers coming in four different options (hereinafter – test items):

− Option 1 – linear density 1.54 g/m, without braid, named Opt.1 for tests at room temperature, Opt.1-1 – for tests at temperature 100°C, Opt.1-2 – for tests at temperature 150°C, Opt.1-3 – for tests at temperature 190°C;

− Option 2 – linear density 3.15 g/m, with braid, named Opt.2 for tests at room temperature, Opt.2-1 – for tests at temperature 100°C, Opt.2-2 – for tests at temperature 150°C, Opt.2-3 – for tests at temperature 190°C;

− Option 3 – linear density 3.10 g/m, without braid, named Opt.3 for tests at room temperature, Opt.3-1 – for tests at temperature 100°C, Opt.3-2 – for tests at temperature 150°C, Opt.3-3 – for tests at temperature 190°C;

− Option 4 – linear density 6.05 g/m, with braid, named Opt.4 for tests at room temperature, Opt.4-1 – for tests at temperature 100°C, Opt.4-2 – for tests at temperature 150°C, Opt.4-3 – for tests at temperature 190°C.[15]

All the tests are conducted at Instron-8801 testing unit with the use of special clamps (Figure 6). For every sample several loadings with subsequent unloadings at room temperature were performed, and then every sample of every type was tested to destruction at room temperature. For the rest of the samples after the loading at room temperature loadings with

subsequent unloadings at preset increased temperature and loadings to destruction at this temperature were performed.

Main numerical results of the tests are provided hereinafter (Table 2 – Table 5). The first column here features the numbers of samples, where the first figure corresponds to the number of the yarn design option, and the second one stands for the level of the testing temperature. There is no second figure for the samples tested to destruction at room temperature. The second column features the number of loading, for which the experimental data is provided forthwith. Here it can be seen that for different samples the number of loadings at room temperature changed from two to nine. The increased number of loadings was related to malfunctions of the strainmeter.

These malfunctions were caused by unwinding of the samples under tension which caused the displacement of the strainmeter knife edge from the initial position as well as the redistribution of the load among certain threads. The degree of this effect manifestation turned out to be different for different samples, but most often it was observed for samples from the thicker yarns of Options 2 and 4.

In the third column the value of maximum load Pmax for each loading is provided. For tests to destruction at room temperature (samples Opt.1, Opt.2, Opt.3, Opt.4) loadings for defining hardness were conducted at Pmax about 2 кН, for the rest of the hardness tests the Pmax value was decreased so as to diminish the possible impact on strength at increased temperature of pre-loadings.

Pmax value for the last loadings stands for the value of loading at the moment of destruction which was registered based on sharp decrease of load which led to the unit shut down. After that the sample maintained some load carrying capacity, which is why in the majority of cases the repeated loadings were conducted till well-observed areas of destruction were formed. Maximum load at repeated loadings were, as a rule, less than the one achieved initially, but sometimes a little higher, too. In this case two critical loads values are provided.

In the fourth column the value of average loadings in the yarn threads is provided, this value is defined by maximum loading divided by the nominal area of the yarn fibers cross-section:

$$S_F = \frac{V_F}{L_Y} = \frac{V_F \rho_{Th}}{L_Y \rho_{Th}} = \frac{M_F}{L_Y \rho_{Th}} = \frac{T_Y}{\rho_{Th}} \qquad (1)$$

where S_F – cross-section of fibers in one yarn; V_F – volume of fibers in the yarn which length is L_Y, ρ_{Th} – volumetric density of the thread material; M_F – mass of the fibers in the yarn which length is L_Y, T_Y – linear density of the yarn.

Here the dimensions of values T_Y and ρ_{Th} shall be such so that S is in square millimeters.

For Options 1 and 3 yarns (without taking into account the braid) this area equals to 1.10 mm^2, and for Options 2 and 4 yarns (without taking into account the braid) - to 2.25 mm^2.

In the following column the deformation values based on strainmeter at P_{max} are provided. Since for loadings to destruction the strainmeter was removed in order to prevent the damage at the moment of destruction, these deformation values are not provided for the last loadings. As a rule, at first loading ε_{max} is measurably higher that at subsequent loadings. This provides important information on the character of the yarns deformation: at first loading threads in yarns undergo maximum straightening and stretching. Since at first loading ε_{max} significantly varies even for the samples of one and the same yarn, it is possible to assume that there is a dispersion of the average degree of the threads tensioning with regard to the yarns length. That is why areas with different average degree of initial tensioning can be observed within the strainmeter base of 25 mm (distances between the prisms attached to the sample). Further on, the tables feature Δ_{max} values – the values of mutual displacement of clamps at P_{max}. Notably, at the first loading this variable has also (like ε_{max}) a higher value (its zero-based count is performed at each loading). The level of Δ_{max} differences for different samples, even for samples from one and the same yarn, is even higher than for ε_{max}. Evidently, apart from fluctuations of average degree of samples threads tensioning, Δ_{max} is also influenced by random fluctuations of yarns tensioning degree during winding on the unit for fastening. (Figure 6).

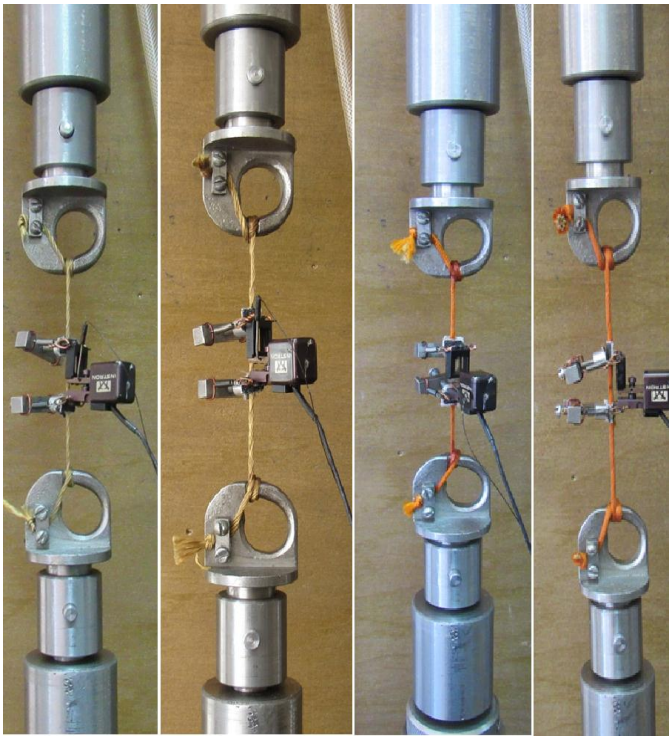

Figure 6. The samples of ropes made of polymer materials prior to testing at room temperature

In the next-to-last column the values of local modules are provided. These values are defined for the majority of loadings for two areas: E_{Th} – at loadings less than 0,5 P_{max}, and E_k – at loadings more than 0.5 P_{max}, since the majority of the dependencies of deformations from loadings are significantly non-linear. If for some loading one modulus value is provided, it means that the dependency of deformations from loading for this test is close to linear for

the whole area of loading. Modules are defined by linear approximation of experimental dependencies with the use of the least-square method. Average threads tensioning values are defined by loading divided by average cross-section of yarn threads:

$$E = \frac{\Delta P}{S_{Th}\Delta\varepsilon}, \qquad (2)$$

there $\Delta P/\Delta\varepsilon$ stands for increment of loadings and deformations along the approximating lines, S_{Th} – in accordance with (1).

At the same time the value of 1.54 g/m was taken as linear density for yarns of Options 1 and 3, and the value of 3.15 g/m for yarns of Options 2 and 4, i.e. the linear density values provided in the supporting documentation for yarns without braids were used. It means that the impact of braid in the module and tensile strength was considered negligibly small. In addition, the linear density values which were used correspond to the threads in winding, i.e. for straightened threads the linear stiffness values would be less, which means that the average calculated cross-section would be less.

The cross-section was determined using the condition: the thread material density ρ_Y=1.4 g/cm^3 – the value, typical for Armos material. In this case there results: S_1 = 1.10 mm^2 for yarns of Options 1 and 3, S_2=2.25 mm^2 for yarns of Options 2 and 4.

RESULTS

The results of the tests on defining the Coefficient of Linear Thermal Expansion of the load-bearing rod elements are provided in Table 1.

Table 1. The results of the tests on defining the Coefficient of Linear Thermal Expansion of the power rod elements

No.	Parameter, designation and the unit of measurement	Design type and sample number	Measured value	
			-30°C	+60°C
1.	CLTE $\alpha_x\cdot10^{-7}$, 1/°C	Design 1, sample No. 1	6.46	9.35
2.	CLTE $\alpha_y\cdot10^{-7}$, 1/°C		13.30	31.40
3.	CLTE $\alpha_x\cdot10^{-7}$, 1/°C	Design 1, sample No. 2	6.55	6.37
4.	CLTE $\alpha_y\cdot10^{-7}$, 1/°C		9.55	28.60

In the last columns the temperature values for each loading are provided, whence it follows that all the samples at first were loaded at room temperature, and then 3 samples of each option at a time were loaded at increased temperature – first to little loading with subsequent unloading, then – to destruction (Table 2 – Table 5). Prior to loading the samples were hold at preset temperature for 6 – 7 minutes. The time of chamber heating up to 100°C amounted to ~ 5 minutes, to 150°C – ~ 8 minutes, to 190°C – ~ 14 minutes.

Table 2-5 features the results of Armos yarn testing.

Table 2. Main results of Armos yarn testing – Option 1

No.of sample	No.of loading	P_{max}, kN	$\bar{\sigma}_{max}$, GPa	ε_{max}, %	Δ_{max}, mm	$E_н$ / $E_к$, GPa	Testing temperature, °C
Opt.1	1	1.8	1.64	2.23	27.62	46.0 / 75.5	25
	2	1.8		1.57	4.85	75.5/117.7	
	3	1.8		1.40	2.42	82.9/117.5	
	4	2.35	2.14	-	3.89	-	
Opt.1-1	1	1.0	0.91	1.22	4.35	64.6/58.1	25
	2	1.0		0.89	1.26	82.2	
	3	1.0		1.0	4.78	76.7/67.6	100
	4	1.65	1.50	-	5.06	-	
Opt.1-2	1	1.0	0.91	1.15	3.64	63.6	25.6
	2	1.0		0.90	1.28	81.2	
	3	0.8	0.73	0.79	7.02	68.9	150
	4	1.43	1.30	-	12÷15	-	
Opt.1-3	1	1.0	0.91	0.96	2.19	74.8	26.0
	2	1.0		0.84	1.24	86.2	
	3	0.8	0.73	-	-	-	190
	4	0.8		0.62	1.23	87.6	
	5	1.08	0.98	-	2.80	-	

Table 3. Main results of Armos yarn testing – Option 2

No.of sample	No.of loading	P_{max}, kN	$\bar{\sigma}_{max}$, GPa	ε_{max}, %	Δ_{max}, mm	$E_н$ / $E_к$, GPa	Testing temperature, °C
Opt.2	1	2.0	0.89	1.1	5.58	67.3/69.1	26
	2	1.0	0.44	0.61	1.0	65.2/86.0	
	7	2.0	0.89	0.89	1.96	89.9/101.2	
	8	2.0		0.99	1.69	68.6/94.4	
	9	2.0		1.0	1.63	66.3/95.5	
	10	3.53	1.57	-	5.15	-	
	11	3.45	1.53	-	8.87	-	
Opt.2-1	1	1.5	0.67	1.3	5.34	35.2/56.9	26.5
	2	1.5		1.1	3.27	52.6	100
	3	2.89	1.28	-	20.4	-	
	4	3.20	1.42	-	24.5	-	
Opt.2-2	1	1.5	0.67	1.3	19.11	35.6/59.2	25.6
	2	1.5		1.0	1.48	54.3/61.5	
	3	1.0	0.44	0.71	8.51	50.0	150
	4	2.0	0.89	-	12.5	-	
Opt.2-3	1	1.5	0.67	1.7	6.13	30.4/39.3	26
	2	1.5		1.0	1.51	52.7/58.2	
	3	1.5		1.0	1.41	53.2/61.4	190
	4	1.0	0.44	0.9	1.85	40.0	
	5	2.54	1.13	-	30.2	-	

Table 4. Main results of Armos yarn testing – Option 3

No.of sample	No.of loading	P_{max}, kN	$\bar{\sigma}_{max}$, GPa	ε_{max}, %	Δ_{max}, mm	$E_н$ / $E_к$, GPa	Testing temperature, °C
Opt.3	1	1.89	1.72	1.8	11.5	70.2/89.3	24
	2	1.8	1.64	1.3	2.3	81.3/122	
	3	1.0	0.91	0.9	1.03	80.0	
	4	2.26	2.05	-	3.45	-	
Opt.3-1	1	1.0	0.91	1,1	5.0	72.0	23
	2	1.0		0.94	1.37	74.8/79.6	
	3	1.0		1.0	2.08	72.4	100
	4	2.11	1.91	-	10.4	-	
Opt.3-2	1	1.0	0.91	2.2	11.5	30.7/52.5	25
	2	1.0		1.1	1.48	68.9	
	3	1.0		1.0	1.36	72.8	
	4	0.8	0.73	0.89	10.92	-60.5	150
	5	1.98	1.80	-	12.5	-	
Opt.3-3	1	1.0	0.91	1.0	4.33	69.7	26.0
	2	1.0		0.83	1.36	88.7	
	3	1.0		0.8	1.28	90.7	
	4	0.8	0.73	0.7	18.35	70.0/71.3	190
	5	0.8		0.68	1.29	79.1	
	6	1.88	1.71	-	14.9	-	

Table 5. Main results of Armos yarn testing – Option 4

No.of sample	No.of loading	P_{max}, кН	$\bar{\sigma}_{max}$, GPa	ε_{max}, %	Δ_{max}, mm	$E_н$ / $E_к$, GPa	Testing temperature, °C
Opt.4	1	2.0	0.89	3.6	19.55	12.3/36.3	25
	2	2.0		1.3	1.99	39.9/63.4	
	3	2.0		1.5	1.72	40.6/63.6	
	4	2.0		1.5	1.69	44.5/63.9	
	5	2.71	1.20	-	3.52	-	
	9	2.92	1.30	-	7.33	-	
Opt.4-1	1	1.5	0.67	3.0	14.51	17.3/23.7	25
	2	1.5		1.2	2.03	40.3/55.5	
	3	1.5		1.5	7.26	38.9	100
	4	3.31	1.47	-	13.7	-	
Opt.4-2	1	1.5	0.67	2.3	10.58	19.2/35.2	24
	2	1.5		1.3	1.91	38.2/46.0	
	3	1.5		1.2	1.54	38.9/53.7	
	4	1.0	0.44	0.91	19.00	26.1/44.4	150
	5	1.0		0.66	2.94	53.1	
	6	2.61	1.16	-	18.3	-	
4-3	2	1.5	0.67	0.50	1,8	72.5/111.2	25
	3	1.0	0.44	0.61	6.1	45.4/74.9	190
	6	1.0		0.60	1.5	48.5/66.8	
	7	2.30	1.02	-	13.0	-	

CONCLUSION

The objective of this research was to define the appropriate options of samples design among the strength rod elements out of the two design options, to define the best design of the yarn with regard to tensile strength at different temperatures, which makes this study unique.

During this study the investigation tests of the structure members of large-sized reconfigurable spacecraft antenna reflectors were conducted. Based on the results of investigation tests of the structure members of large-sized reconfigurable spacecraft antenna reflectors both design options of strength rod element are feasible for operation in space environment for large-sized reflector and provide for required precision of the reflector's reflecting surface, since it is the Coefficient of Linear Thermal Expansion which is a limiting parameter of temperature deformations of the indicated structure members. It is the CLTE which determines the temperature deformations of the most extended structure members of the reflector. With this regard the structure of reinforcement of the carbon composite rods is selected in such a way as to minimize the CLTE. All the design options of ropes are also feasible for using them in the reconfigurable antenna reflector structure. The rigidity of ropes used for network curtain tensioning also has a significant impact on the quality of the reflecting surface.

ACKNOWLEDGEMENTS

Some results presented hereby were obtained under the Grant Contract No. 14.577.21.0129 of October 28, 2014 with the Ministry of Education and Science of the Russian Federation. Unique identifier of applied research (project) is RFMEFI57714X0129.

REFERENCES

[1] Jiang J, Li T, Ma X, Wang P. A nonlinear equivalent circuit method for analysis of passive intermodulation of mesh reflectors. Chinese Journal of Aeronautics. 2014, 27(4), 924-929. DOI: 10.1016/j.cja.2014.03.003

[2] Li TJ, J. Jiang J, Deng HQ, Lin ZC, Wang ZW. Form-finding methods for deployable mesh reflector antennas. Chinese Journal of Aeronautics. 2013; 26(5), 1276–1282. DOI: 10.1016/j.cja.2013.04.062

[3] Chugui YuV, Skokov DV, Khalimanovich VI, Verkhoglyad AG, Nakrokhin IA. A mechanism for telescopic extension of reflector's tubular spokes and shafts. Reshetnev Readings. 2015; 1(19), 141-143. Available at: http://elibrary.ru/item.asp?id=271264164.

[4] Gerasimov AV, Zhukov AP, Ponomarev VS, Ponomarev SV, Halimanovich VI. Simulation of large deployable wrap-rib reflector. Reshetnev Readings. 2014; 1(18), 68-69

[5] Frizelle WG. Injection Molding Technology. In: Applied Plastics Engineering Handbook (Second Edition), 2011, 191-202. DOI: 10.1016/B978-1-4377-3514-7.10013-3.

[6] Mishra SK, Kumar V, Tiwari SK, Mishra T, Angula G, Adhikari S. Development and degradation behavior of protective multilayer coatings for aluminum reflectors for solar thermal applications. Thin Solid Films. 2016, 619, 202-207. .DOI: 10.1016/j.tsf.2016.10.067

[7] García-Segura A, Fernández-García A, Ariza MJ, Sutter F, Valenzuela L. Durability studies of solar reflectors: A review. Renewable and Sustainable Energy Reviews. 2016, 62, 453-467. DOI: 10.1016/j.rser.2016.04.060

[8] Yu G-C, Wu L-Z, Feng L-J, Yang W. Thermal and mechanical properties of carbon fiber polymer-matrix composites with a 3D thermal conductive pathway. Composite Structures, 2016. 149, 213-219. DOI: 10.1016/j.compstruct.2016.04.010

[9] Zhao Y-H, Zhang Y-F, Bai S-L, Yuan X-W. Carbon fibre/graphene foam/polymer composites with enhanced mechanical and thermal properties. Composites Part B: Engineering, 2016, 94, 102-108. DOI: 10.1016/j.compositesb.2016.03.056

[10] Raghubanshi H, Dikio ED, Naidoo EB. The properties and applications of helical carbon fibers and related materials: A review. Journal of Industrial and Engineering Chemistry. 2016, 44, 23-42. DOI: 10.1016/j.jiec.2016.08.023

[11] Arnaout M, Paulmier T, Dirassen B, D. Payan D. Study of radiation induced conductivity and photoconduction phenomenon for materials used in space environment // Journal of Electrostatics. 2016, 84, 48-53. DOI: 10.1016/j.elstat.2016.09.001

[12] Paglia L, Tirillò J, Marra F, Bartuli C, Simone A, Valente T, Pulci G. Carbon-phenolic ablative materials for re-entry space vehicles: plasma wind tunnel test and finite element modeling. Materials & Design. 2016, 90, 1170-1180. DOI: 10.1016/j.matdes.2015.11.066

[13] Beloglazov AP, Gabov AV, Yelistratov VI. Prospects of mandrels designing with small thermal expansion coefficient for manufacturing reflectorS. Reshetnev Readings. 2014, 1, 18, 49-50. http://elibrary.ru/item.asp?id=22482579 Date accessed: 12.07.2016.

[14] Tairova L.P., Shapkina V.M. Study of Peculiarities of Deforming of Cross-Reinforced Carbon-Filled Plastic Plates with Temperature Change Using Tensometric Means. Newsletter of Bauman Moscow State Technical University. Series: Mechanical Engineering. 2011, SP, 61-68. http://cyberleninka.ru/article/n/issledovanie-osobennostey-deformirovaniya-ugleplastikovyh-perekrestno-armirovannyh-plastin-pri-izmenenii-temperatury-sredstvami. Date accessed: 12.07.2016.

[15] Arzamasov IV. Applying molded plastics in modern mechanical engineering. In: Education, Science, Production. Belgorod, 2015 – pp. 1604-1608. http://elibrary.ru/item.asp?id=25571709